Available online at www.sciencedirect.com
SCIENCE DIRECT®
Communications in Nonlinear Science and Numerical Simulation 11 (2006) 934–960
Communications in Nonlinear Science and Numerical Simulation
www.elsevier.com/locate/cnsns

Stability of synchronized dynamics and pattern formation in coupled systems: Review of some recent results

Yonghong Chen [a,*], Govindan Rangarajan [b,c], Mingzhou Ding [a]

[a] *Department of Biomedical Engineering, University of Florida, 120 BME Building/P.O. Box 116131, Gainesville, FL 32611, USA*
[b] *Department of Mathematics and Centre for Theoretical Studies, Indian Institute of Science, Bangalore 560 012, India*
[c] *Jawaharlal Nehru Centre for Advanced Scientific Research, Bangalore 560 012, India*

Received 18 January 2005; received in revised form 21 January 2005; accepted 24 January 2005
Available online 12 March 2005

Abstract

In arbitrarily coupled dynamical systems (maps or ordinary differential equations), the stability of synchronized states (including equilibrium point, periodic orbit or chaotic attractor) and the formation of patterns from loss of stability of the synchronized states are two problems of current research interest. These two problems are often treated separately in the literature. Here, we present a unified framework in which we show that the eigenvalues of the coupling matrix determine the stability of the synchronized state, while the eigenvectors correspond to patterns emerging from desynchronization. Based on this simple framework three results are derived: First, general approaches are developed that yield constraints directly on the coupling strengths which ensure the stability of synchronized dynamics. Second, when the synchronized state becomes unstable spatial patterns can be selectively realized by varying the coupling strengths. Distinct temporal evolution of the spatial pattern can be obtained depending on the bifurcating synchronized state. Third, given a desired spatiotemporal pattern, one is able to design coupling schemes which give rise to that pattern as the coupled system evolves. Systems with specific coupling schemes are used as examples to illustrate the general methods.

* Corresponding author. Tel.: +1 352 392 0635; fax: +1 352 392 9791.
E-mail addresses: ychen@bme.ufl.edu (Y. Chen), rangaraj@math.iisc.ernet.in (G. Rangarajan), ding@bme.ufl.edu (M. Ding).

1007-5704/$ - see front matter © 2005 Elsevier B.V. All rights reserved.
doi:10.1016/j.cnsns.2005.01.011

PACS: 05.45.Xt; 89.75.Kd; 07.05.Mh

Keywords: Coupled dynamical systems; Chaotic synchronization; Generalized Turing patterns

1. Introduction

Large arrays or networks of coupled dynamical systems have attracted increasing interest due to their wide application potential in the study of natural and engineering systems. From biology to engineering, coupled map or coupled oscillator models have played considerable roles in revealing the functional mechanism underlying phenomena such as synchronization/coordination, and the formation of complex patterns [20,21,40,54,33,34,47,39,55,56,36,11]. The essential problems concerned are usually to know the extent to which the coupling strengths can be varied so that the synchronized state remains stable and how to vary the coupling strengths in order to realize some spatial patterns once the synchronized state becomes unstable. Early work has typically looked at the two problems in systems of very small size or in systems with very specific coupling schemes (diffusive coupling, global all to all coupling etc. with a single coupling strength) [14,51,38,6,22,31,5,48,4,18,2,3,30,10,17,58,28]. Recent work introduced the notion of a master stability function that enables the analysis of general coupling topologies [42,12]. This function defines a region of stability in terms of the eigenvalues of the coupling matrix [27,57]. However, no explicit constraints on coupling strengths themselves were given. Another area of great interest in coupled systems is the study of Generalized Turing Patterns (GTPs). These patterns differ from the classic Turing patterns [50] in the following sense. Whereas classical Turing patterns emerge from homogeneous equilibrium states, the GTPs emerge from global synchronized limit cycles or chaotic states. Moreover, the underlying coupled system need not have diffusive coupling. The GTPs have been the subject of several recent publications [23,41]. These papers mainly rely on numerical techniques to obtain the threshold of instabilities and no general method to realize a given GTP is given.

In this paper we focus on providing a unified approach toward the problem of stability and pattern formation in coupled systems by tying together several recent results that have addressed the question of stability and the question of pattern formation separately [8,45,49]. The paper is organized as follows. In Section 2 we introduce the general mathematical framework and the notion of a master stability function. In Section 3, by combining the master stability function and the Gershgorin disc theorem, we derive explicit constraints on the coupling strengths which give the stability zone of the synchronized dynamics. We analyze both equilibrium synchronized states and chaotic synchronized states. In Section 4, we compare the stability regions obtained by the method in Section 3 and by the exact solution for systems where such solutions are possible. In Section 5, we show how the coupling strengths can be varied along specific paths in the parameter space to selectively realize admissible GTPs for that system. Moreover, given a desired GTP, we present a general method to design a coupled dynamical system that would give rise to this pattern under time evolution. Our methods are applicable to both coupled maps and coupled ordinary differential equations (ODEs). Commonly studied coupling schemes are used as illustrative examples.

2. General stability region

The first step towards a general stability analysis of coupled identical systems is the linear eigenvalue analysis around a given solution. In the following we carry out this analysis for both coupled maps and coupled ODEs.

2.1. Coupled maps

The system we consider is represented by

$$\mathbf{x}^i(n+1) = \mathbf{f}(\mathbf{x}^i(n)) + \frac{1}{N}\sum_{j=1}^{N} G_{ij}\cdot \mathbf{H}(\mathbf{x}^j(n)), \tag{1}$$

where $\mathbf{x}^i(n)$ is the M-dimensional state vector of the ith map at time n and $\mathbf{H}: R^M \to R^M$ is the coupling function. We define $\mathbf{G} = [G_{ij}]$ as the coupling matrix where G_{ij} gives the coupling strength from map j to map i.

We are interested in the linear stability of the synchronized state $\mathbf{x}(n)$ (additional conditions may be needed to ensure that $\mathbf{x}(n)$ is a solution of the system and these will be addressed later). The synchronized state defines the synchronization manifold in the phase space of the system. Linearizing Eq. (1) around the synchronized state, which evolves according to $\mathbf{x}(n+1) = \mathbf{f}(\mathbf{x}(n))$, we have

$$\mathbf{z}^i(n+1) = \mathbf{J}(\mathbf{x}(n))\cdot \mathbf{z}^i(n) + \frac{1}{N}\sum_{j=1}^{N} G_{ij}\cdot D\mathbf{H}(\mathbf{x}(n))\cdot \mathbf{z}^j(n), \tag{2}$$

where $\mathbf{z}^i(n)$ denotes the ith map's deviations from $\mathbf{x}(n)$, $\mathbf{J}(\cdot)$ is the $M\times M$ Jacobian matrix for $\mathbf{f}$ and $D\mathbf{H}(\cdot)$ is the Jacobian of the coupling function $\mathbf{H}$. In terms of the $M\times N$ matrix $\mathbf{S}(n) = (\mathbf{z}^1(n)\mathbf{z}^2(n)\cdots\mathbf{z}^N(n))$, Eq. (2) can be recast as

$$\mathbf{S}(n+1) = \mathbf{J}(\mathbf{x}(n))\cdot \mathbf{S}(n) + \frac{1}{N} D\mathbf{H}(\mathbf{x}(n))\cdot \mathbf{S}(n)\cdot \mathbf{G}^{\mathrm{T}}. \tag{3}$$

The linear stability of Eq. (3) is determined by the eigenvalue λ of $\mathbf{G}$. Denote the corresponding eigenvector by $\mathbf{e}$ and let $\mathbf{u}(n) = \mathbf{S}(n)\mathbf{e}$ where we have suppressed the dependence on λ for notational simplicity. Then

$$\mathbf{u}(n+1) = \left(\mathbf{J}(\mathbf{x}(n)) + \frac{1}{N}\lambda\cdot D\mathbf{H}(\mathbf{x}(n))\right)\cdot \mathbf{u}(n) \quad \text{for each } \lambda. \tag{4}$$

We note that the stability problem originally formulated in the $M\times N$ space has been reduced to a problem in a $M\times M$ space where it is often the case that $M \ll N$. Next, we calculate the Lyapunov exponents (which depend on λ) from the above equation. If all Lyapunov exponents transverse to the synchronization manifold are negative, the synchronized state is stable since any deviation away from the synchronized manifold will quickly die down. Using this condition, we later obtain constraints on the coupling strengths which will ensure stability of the synchronized state.

2.2. Coupled ODEs

The above procedure for reducing the original $M \times N$ space problem to a $M \times M$ space can also be applied to coupled identical ODEs written as

$$\dot{\mathbf{x}}^i = \mathbf{F}(\mathbf{x}^i) + \frac{1}{N}\sum_{j=1}^{N} G_{ij}\mathbf{H}(\mathbf{x}^j), \tag{5}$$

where $\mathbf{x}^i$ is the M-dimensional vector of the ith node. Linearizing around the synchronized state $\mathbf{x}$ (which evolves according to the equation $\dot{\mathbf{x}} = \mathbf{F}(\mathbf{x})$) we get

$$\dot{\mathbf{z}}^i = \mathbf{J}(\mathbf{x}) \cdot \mathbf{z}^i + \frac{1}{N}\sum_{j=1}^{N} G_{ij} \cdot D\mathbf{H}(\mathbf{x}) \cdot \mathbf{z}^j, \tag{6}$$

where $\mathbf{z}^i$ denotes deviations from $\mathbf{x}$, $\mathbf{J}(\cdot)$ and $D\mathbf{H}(\cdot)$ are the $M \times M$ Jacobian matrices for the functions of $\mathbf{F}$ and $\mathbf{H}$. Adopting Jordan canonical form, we obtain

$$\dot{\mathbf{u}} = \left[\mathbf{J}(\mathbf{x}) + \frac{1}{N}\lambda \cdot D\mathbf{H}(\mathbf{x})\right]\mathbf{u}, \tag{7}$$

where λ is an eigenvalue of $\mathbf{G}$. It is worth mentioning that this eigenvalue based analysis is valid even if the coupling matrix $\mathbf{G}$ is defective [24]. As before, if all the transverse Lyapunov exponents are negative, the synchronized state is stable.

In both the cases studied above, stability was characterized in terms of Lyapunov exponents. We can formulate this in terms of the eigenvalues of G (the coupling matrix) as follows. Treat λ in Eq. (4) or (7) as a complex parameter and calculate the maximum Lyapunov exponent $\mu_{\max}$ as a function of λ. This is referred to as the master stability function by Pecora and Carroll [42]. The region in the (Re(λ), Im(λ)) plane where $\mu_{\max} < 0$ defines a stability region denoted by Ω. If the transverse eigenvalues of the coupling matrix are within Ω, then the synchronized state is stable.[1] By transverse eigenvalues we mean those eigenvalues in Eq. (4) or (7) which correspond to dynamics in the manifold transverse to the synchronization manifold. Fig. 1 shows a schematic of two possible configurations of Ω. Whether Ω is an unbounded area [Fig. 1(a)] or a bounded one [Fig. 1(b)] is contingent on the coupling scheme and other system parameters. We note that, typically, Ω is obtained numerically. In some instances analytical results are possible (see below).

3. Stability constraints on coupling strengths

Stability region Ω gives constraints on the eigenvalues of the coupling matrix which ensure the stability of the synchronized state. Here, we seek constraints applicable directly on the coupling strengths. This problem is dealt with by combining the master stability function with the Gershgörin disc theory.

[1] We note that, since the Lyapunov exponent $h_{\max}$ is computed from typical initial conditions, the stability here is with respect to the blowout bifurcation. Bubbling transition can occur while the parameters are still within the bound derived in this work. For details on these phenomena, see [59–62].

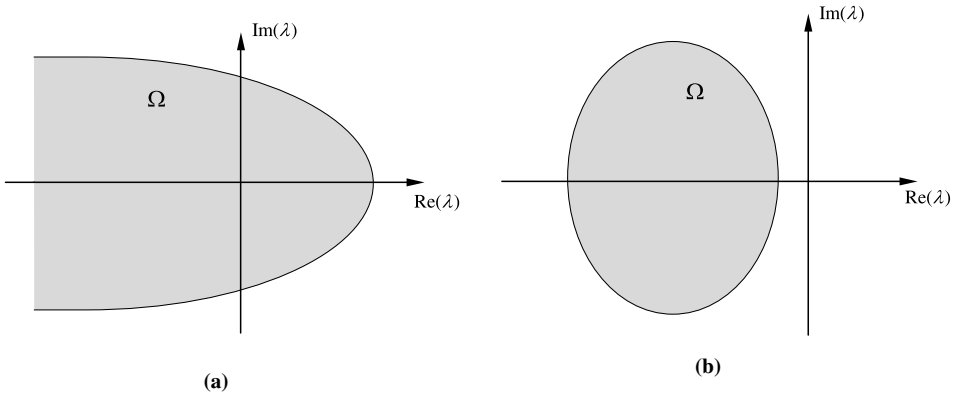

Fig. 1. Schematic illustrations of the stability region: (a) unbounded area, (b) bounded area.

The Gershgörin disc theorem [26] states that all the eigenvalues of a $n \times n$ matrix $\mathbf{A} = [a_{ij}]$ are located in the union of n discs (called Gershgörin discs) where each disc is given by

$$\left\{ z \in C : |z - a_{ii}| < \sum_{j \neq i} |a_{ji}| \right\}, \quad i = 1, 2, \ldots, n. \tag{8}$$

Before applying this theorem, let us consider conditions which ensure that the synchronized state is a solution of the coupled system (1) or (5). In systems such as neural networks, the synchronized state is an equilibrium state and we want it to be stable even after the individual systems are coupled together [25,52,1,32,35,53,13]. In this case the origin can be taken to be the equilibrium point without loss of generality and the condition $\mathbf{H}(\mathbf{x}) = \mathbf{0}$ needs to be imposed in order to make it a solution of the coupled system. On the other hand, when the individual system is chaotic, the condition $\sum_{j=1}^{N} G_{ij} = 0$ is imposed to ensure that the synchronized state is a solution. The Gershgörin disc theorem has to be applied in different ways for these two cases.

3.1. Synchronization of equilibrium states

When the synchronized state is an equilibrium point, the synchronization manifold reduces to a point, and all eigenvalues of the coupling matrix in Eq. (1) or (5) contribute to the transverse dynamics. Therefore, if all the Gershgörin discs are restricted to lie within the stability region, the synchronized equilibrium state will be stable.

Besides Eq. (8), the n Gershgörin discs can also be written in the following alternative forms [26]:

$$\left\{ z \in C : |z - a_{ii}| \leqslant \sum_{j \neq i} |a_{ij}| \right\}, \quad i = 1, 2, \ldots, n.$$

Combining the two forms of Gershgörin discs, we have the following form which is particularly suited for neural network models:

$$\left\{ z \in C : |z - a_{ii}| \leqslant \frac{1}{2} \sum_{j \neq i} (|a_{ji}| + |a_{ij}|) \right\}, \quad i = 1, 2, \ldots, n. \tag{9}$$

This form is more intuitive since it involves both incoming and outgoing coupling strengths for a given node. Applying Gershgörin disc theorem, the stability conditions for the equilibrium point can now be stated as follows:

(1) The center G_{ii} ($i = 1, 2, \ldots, N$) of every Gershgörin disc of $\mathbf{G}$ lies inside the stability zone Ω.
(2) The radius of every Gershgörin disc is shorter than the distance from the center of that disc to the boundary of Ω.

Let $\delta(x)$ denote the distance from a point x on the real axis to the boundary of Ω. Then the stability of the equilibrium point is ensured if

$$(G_{ii}, 0) \in \Omega \quad \text{and} \quad \frac{1}{2} \sum_{j \neq i} (|G_{ji}| + |G_{ij}|) < \delta(G_{ii}) \tag{10}$$

for $i = 1, 2, \ldots, N$.

In the following, we obtain analytical results for specific neural network models.

3.1.1. One-dimensional system

When one-dimensional systems are coupled together, the matrices $D\mathbf{F}$ and $D\mathbf{H}$ reduce to real numbers. Representing them by μ and v, respectively, the stability zone is easily obtained as $\mathrm{Re}(\lambda) < -\mu/v$. The distance from the center of the ith Gershgörin disc to the boundary of Ω is given by $\delta(G_{ii}) = -\mu/v - G_{ii}$. Using Eq. (10) we obtain the stability conditions as

$$\frac{1}{2} \sum_{j \neq i} (|G_{ji}| + |G_{ij}|) + G_{ii} < -\mu/v. \tag{11}$$

This result was obtained before in [25,52].

3.1.2. Two-dimensional coupled oscillator model

Let us consider a network whose functional unit is a cortical column consisting of mutually coupled excitatory and inhibitory populations [1,32,35,53,13]. The columns are coupled through mutually excitatory interactions to form the network.

A single column is described by two first-order differential equations

$$\begin{aligned} \frac{\mathrm{d}x}{\mathrm{d}t} + ax &= -k_{ei} Q(y, Q_m) + I, \\ \frac{\mathrm{d}y}{\mathrm{d}t} + by &= k_{ie} Q(x, Q_m). \end{aligned} \tag{12}$$

Here, x, y represent the local field potentials of the excitatory and inhibitory populations, respectively, and I is the input ($I = 0$ in the subsequent analysis). The constants a, $b > 0$ are the damping constants. The parameter $k_{ie} > 0$ gives the coupling gain from the excitatory (x) to the inhibitory

(y) population whereas $k_{ei} > 0$ represents the strength of the reciprocal coupling. We use a sigmoid coupling function for Q and we only need to specify that $Q(0, Q_m) = 0$ and $Q'(0, Q_m) = 1$.

The N columns are coupled together in the following fashion:

$$\begin{aligned} \frac{dx_n}{dt} + ax_n &= -k_{ei}Q(y_n, Q_m) + \frac{1}{N}\sum_{p=1}^{N} c_{np}Q(x_p, Q_m) + I_n, \\ \frac{dy_n}{dt} + by_n &= k_{ie}Q(x_n, Q_m), \end{aligned} \tag{13}$$

where the columns are indexed by $n = 1,2,\ldots,N$ and the coupling strength c_{np} is the gain from the excitatory population of column p to the excitatory population of column n.

Here, the synchronized equilibrium is $(0,0)$. Linearizing the above system about this state we obtain Eq. (7) where

$$\mathbf{J} = \begin{pmatrix} -a & -k_{ei} \\ k_{ie} & -b \end{pmatrix}, \quad \mathbf{G} = [c_{np}], \quad D\mathbf{H} = \begin{pmatrix} 1 & 0 \\ 0 & 0 \end{pmatrix}.$$

Here, we have used the fact $Q'(0, Q_m) = 1$.

Applying the generalized Routh–Hurwitz criterion [16] to analyze the eigenvalues of the matrix $(D\mathbf{F} + \frac{\lambda}{N}D\mathbf{H})$, we find the stability region Ω (shown in Fig. 2(a)) to be the region to the left of the following curve (see Appendix A.1 for additional details)

$$\lambda_I^2 = \frac{(N(k_{ei}k_{ie} + ab) - b\lambda_R)(N(a+b) - \lambda_R)^2}{b(\lambda_R - Na)}. \tag{14}$$

The pointed tip of the curve in Fig. 2(a) along the real axis is given by $(N\min(a + b, a + k_{ie}k_{ei}/b), 0)$ and it corresponds to the boundary of Ω for the symmetric coupling case. The distance $\delta(G_{ii})$ from the center of the ith Gershgörin disc to the boundary is (see Appendix A.2 for additional details)

$$\delta(G_{ii}) = \sqrt{A_i + 2N\sqrt{B_i}}, \quad i = 1, 2, \ldots, N, \tag{15}$$

where

$$\begin{aligned} A_i &= (Na - G_{ii})^2 - (Nb)^2 - 2N^2k_{ie}k_{ei}, \\ B_i &= Nk_{ie}k_{ei}[2b(N(a+b) - G_{ii}) + Nk_{ie}k_{ei}]. \end{aligned}$$

The stability conditions [cf. Eq. (10)] for the symmetric coupling case are therefore given by

$$G_{ii} < N\min(a + b, a + k_{ie}k_{ei}/b), \quad \frac{1}{2}\sum_{j\neq i}(|G_{ji}| + |G_{ij}|) < \sqrt{A_i + 2N\sqrt{B_i}}, \qquad i = 1, 2, \ldots, N.$$

We note that since the boundary curve of the stability region asymptotically approaches the straight line $\lambda_R = Na$, we can approximate the boundary by this line. In this case, we obtain simpler stability constraints as follows. The distance to the new boundary is easily found to be

$$\delta_i = |Na - G_{ii}| \tag{16}$$

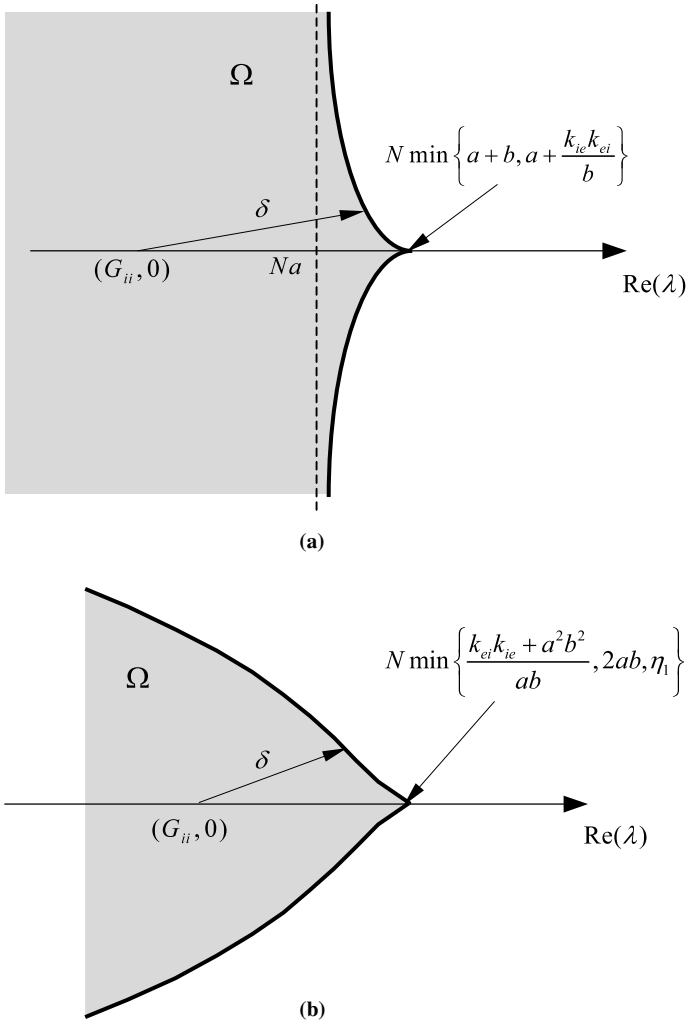

Fig. 2. Stability region of synchronized equilibrium points: (a) a neural network model with $M = 2$, (b) a neural network model with $M = 4$.

and the stability condition simplifies to

$$\frac{1}{2}\sum_{j\neq i}(|G_{ji}| + |G_{ij}|) + G_{ii} < Na, \quad i = 1, 2, \ldots, N. \tag{17}$$

This simplified condition is a good approximation if $\min(a + b, a + k_{ie}k_{ei}/b)$ is sufficiently close to a. We further note that Eq. (17) is satisfied if

$$|G_{ij}| < a, \quad i, j = 1, 2, \ldots, N.$$

That is, the equilibrium point is stable if

$$|c_{np}| < a \quad \forall\, n, p = 1, 2, \ldots, N.$$

This simple stability bound on the individual coupling strengths can be very useful in practice.

3.1.3. Example of a four-dimensional coupled oscillator model

The previous model represents a neural population using first-order differential equations. This has the property that its impulse response has a instantaneous rise phase. Here, we consider another model where the neural population is modelled using second-order differential equations possessing a finite rise and decay impulse response. Each individual column is described by a system of two second-order differential equations [13]:

$$\begin{aligned}\frac{d^2x}{dt^2} + (a+b)\frac{dx}{dt} + abx &= -k_{ei}Q(y, Q_m) + I,\\ \frac{d^2y}{dt^2} + (a+b)\frac{dy}{dt} + aby &= k_{ie}Q(x, Q_m).\end{aligned} \tag{18}$$

The parameters have the same interpretation as before. The N column equations are given by

$$\begin{aligned}\frac{d^2x_n}{dt^2} + (a+b)\frac{dx_n}{dt} + abx_n &= -k_{ei}Q(y_n, Q_m) + \frac{1}{N}\sum_{p=1}^{N} c_{np}Q(x_p, Q_m) + I_n,\\ \frac{d^2y_n}{dt^2} + (a+b)\frac{dy_n}{dt} + aby_n &= k_{ie}Q(x_n, Q_m).\end{aligned} \tag{19}$$

We first consider the stability of the single column equations given in Eq. (18). When the input I is zero, the origin $x = 0$, $y = 0$ is an equilibrium point. In order to study its stability properties, we convert the above second-order differential equations to the following system of first-order differential equations:

$$\begin{aligned}\frac{dz_1}{dt} &= z_2,\\ \frac{dz_2}{dt} &= -(a+b)z_2 - abz_1 - k_{ei}Q(z_3, Q_m),\\ \frac{dz_3}{dt} &= z_4,\\ \frac{dz_4}{dt} &= -(a+b)z_4 - abz_3 + k_{ie}Q(z_1, Q_m),\end{aligned}$$

where

$$z_1 = x, \quad z_2 = \frac{dx}{dt}, \quad z_3 = y, \quad z_4 = \frac{dy}{dt}.$$

The Jacobian matrix $\mathbf{J}$ is obtained as

$$\mathbf{J} = \begin{pmatrix} 0 & 1 & 0 & 0\\ -ab & -(a+b) & -k_{ei} & 0\\ 0 & 0 & 0 & 1\\ k_{ie} & 0 & -ab & -(a+b)\end{pmatrix}. \tag{20}$$

Here, we have used the fact that $Q'(0, Q_m) = 1$. For stability of the origin, the real parts of all eigenvalues of $\mathbf{J}$ should be less than zero. The eigenvalues are determined from the characteristic equation:

$$\lambda^4 + 2(a+b)\lambda^3 + (a^2 + 4ab + b^2)\lambda^2 + 2(a^2 b + ab^2)\lambda + k_{ie}k_{ei} + a^2 b^2 = 0.$$

Applying the Lienard–Chipart criterion [16], we get the following condition which ensures that the origin is stable for the single column equations

$$k_{ie}k_{ei} < ab(a+b)^2. \tag{21}$$

Next, we consider the stability of a network of coupled columns given in Eq. (19). Here

$$\mathbf{G} = [c_{np}],$$

and

$$D\mathbf{H} = \begin{pmatrix} 0 & 0 & 0 & 0 \\ 1 & 0 & 0 & 0 \\ 0 & 0 & 0 & 0 \\ 0 & 0 & 0 & 0 \end{pmatrix}.$$

As before, we examine the eigenvalue α of the matrix $\mathbf{J} + \frac{\lambda}{N} \cdot D\mathbf{H}$ as a function of λ. The characteristic polynomial of this matrix is given by

$$f(\alpha) = \alpha^4 + 2(a+b)\alpha^3 + \left[(a+b)^2 + 2ab - \frac{\lambda}{N}\right]\alpha^2 + \left[2ab(a+b) - \frac{\lambda}{N}(a+b)\right]\alpha + \left[a^2 b^2 - ab\frac{\lambda}{N} + k_{ie}k_{ei}\right]. \tag{22}$$

For complex λ, we are not able to obtain an analytical form for the stability zone Ω, since the characteristic equation results in a eighth-order polynomial when applying the generalized Routh–Hurwitz criterion [16]. However, numerical results are always possible. Fig. 2(b) shows the stability region Ω when $a = 0.22$, $b = 0.72$, $k_{ie} = 0.1$, $k_{ei} = 0.4$. After numerically finding the distance $\delta(G_{ii})$ from the center of the ith Gershgörin disc to the boundary curve, Eq. (10) can again be used to give the stability criteria.

If the coupling is symmetric, which implies that λ is real, the stability boundary is just the rightmost tip of the curve along the real axis in Fig. 2(b). Then the distance δ is given by the absolute difference between the coordinates of the tip point $(\kappa, 0)$ and the center of the ith Gershgörin disc. This tip $(\kappa, 0)$ can be determined by applying the Lienard–Chipart criterion as (see Appendix A.3 for details)

$$\kappa = \min\left\{N\frac{k_{ie}k_{ei} + a^2 b^2}{ab}, 2Nab, \eta_1\right\}, \tag{23}$$

where $\eta_1 = N(a+b)^2 + N\sqrt{(a+b)^4 - 4[ab(a+b)^2 - k_{ie}k_{ei}]}$. Therefore, the distance function $\delta(G_{ii})$ is given by

$$\delta(G_{ii}) = |\kappa - G_{ii}|, \quad i = 1, 2, \ldots, N. \tag{24}$$

Applying Eq. (10), we obtain the following stability condition for the present model with symmetric couplings:

$$\frac{1}{2}\sum_{j\neq i}(|G_{ji}|+|G_{ij}|)+G_{ii}\leqslant\kappa,\quad i=1,2,\ldots,N. \tag{25}$$

As we discussed before, this condition is satisfied if the individual coupling strengths obey the following stability constraints:

$$|c_{np}|<\frac{\kappa}{N}\quad\text{for } c_{np}=c_{pn},\ \ n,p=1,2,\ldots,N. \tag{26}$$

3.2. Synchronization of chaotic states

When the synchronized state is chaotic, the condition $\sum_{j=1}^{N}G_{ij}=0$ needs to be imposed as discussed earlier. Then $\lambda=0$ is always an eigenvalue of $\mathbf{G}$ and its corresponding eigenvector is $(1\quad 1\quad\cdots\quad 1)^{\mathrm{T}}$ which is tangential to the synchronization manifold. However, for stability of the synchronized state, we only require the transverse eigenvalues to lie in Ω. Therefore, we need to remove $\lambda=0$ before applying the Gershgörin disc theorem. In other words, for synchronized chaotic systems, the stability region does not include the origin. In order to exclude $\lambda=0$, we appeal to an order reduction technique in matrix theory [19] which leads to a $(N-1)\times(N-1)$ matrix $\mathbf{D}$ whose eigenvalues are the same as the eigenvalues of $\mathbf{G}$ except for $\lambda=0$.

Suppose that, for a given matrix $\mathbf{G}$, we have knowledge of one of its eigenvalues $\tilde{\lambda}$ and the eigenvector $\mathbf{e}$. Through proper normalization we can make any one component of $\mathbf{e}$ equal to one. Here, without loss of generality, we assume that the first component is made equal 1, namely, $\mathbf{e}=(1,\mathbf{e}_{N-1}^{\mathrm{T}})^{\mathrm{T}}$. We rewrite $\mathbf{G}$ in the following block form:

$$\mathbf{G}=\begin{pmatrix}G_{11} & \mathbf{r}^{\mathrm{T}}\\ \mathbf{s} & \mathbf{G}_{N-1}\end{pmatrix} \tag{27}$$

with $\mathbf{r}=(G_{12},\ldots,G_{1N})^{\mathrm{T}}$, $\mathbf{s}=(G_{21},\ldots,G_{N1})^{\mathrm{T}}$ and

$$\mathbf{G}_{N-1}=\begin{pmatrix}G_{22} & \cdots & G_{2N}\\ \vdots & \vdots & \vdots\\ G_{N2} & \cdots & G_{NN}\end{pmatrix}. \tag{28}$$

Choose a matrix $\mathbf{P}$ in the form

$$\mathbf{P}=\begin{pmatrix}1 & \mathbf{0}^{\mathrm{T}}\\ \mathbf{e}_{N-1} & \mathbf{I}_{N-1}\end{pmatrix}. \tag{29}$$

Here, $\mathbf{I}_{N-1}$ is the $(N-1)\times(N-1)$ identity matrix. Similarity transformation of $\mathbf{G}$ by $\mathbf{P}$ yields

$$\mathbf{P}^{-1}\mathbf{G}\mathbf{P}=\begin{pmatrix}\tilde{\lambda} & \mathbf{r}^{\mathrm{T}}\\ \mathbf{0} & \mathbf{G}_{N-1}-\mathbf{e}_{N-1}\mathbf{r}^{\mathrm{T}}\end{pmatrix}. \tag{30}$$

Since $\mathbf{P}^{-1}\mathbf{GP}$ and $\mathbf{G}$ have identical eigenvalue spectra, the $(N-1)\times(N-1)$ matrix

$$\mathbf{D}^1 = \mathbf{G}_{N-1} - \mathbf{e}_{N-1}\mathbf{r}^{\mathrm{T}} \tag{31}$$

assumes the eigenvalues of $\mathbf{G}$ sans $\tilde{\lambda}$. We can obtain N different versions of the reduced matrix, which we denote by $\mathbf{D}^k$ (k = 1,2,...,N), depending on which component of $\mathbf{e}$ is made equal 1.

Applying the above technique to the coupling matrix G by letting $\tilde{\lambda} = 0$ and $\mathbf{e} = (1 \quad 1 \quad \cdots \quad 1)^{\mathrm{T}}$ we get $\mathbf{D}^k = [d_{ij}^k]$ where $d_{ij}^k = G_{ij} - G_{kj}$. From the Gershgörin theorem the stability conditions of the synchronized dynamics are expressed as

(1) the center of every Gershgörin disc of $\mathbf{D}^k$ lies inside the stability zone Ω. That is, $(G_{ii} - G_{ki}, 0) \in \Omega$;
(2) the radius of every Gershgörin disc of $\mathbf{D}^k$ satisfies the inequality

$$\sum_{j=1, j\neq i}^{N} |G_{ji} - G_{ki}| < \delta(G_{ii} - G_{ki}), \quad i = 1, 2, \ldots, N \quad \text{and} \quad i \neq k.$$

As k varies from 1 to N, we obtain N sets of stability conditions. Each set provides sufficient conditions constraining the coupling strengths.

Next we illustrate the general approach by applying the above results to two examples where analytical results are possible.

3.2.1. Coupled ODE

In this example we consider coupled differential equation systems with $\mathbf{H}(\mathbf{x}) = \mathbf{x}$ [27,57]. It is easy to see that $D\mathbf{H}$ is a $M \times M$ identity matrix. The Lyapunov exponents for Eq. (7) are easily calculated since the identity matrix commutes with $\mathbf{J}(\mathbf{x})$. Denoting them by $\mu_1(\lambda)$, $\mu_2(\lambda)$,...,$\mu_M(\lambda)$, we have

$$\mu_i(\lambda) = h_i + \frac{1}{N} Re(\lambda), \quad i = 1, 2, \ldots, M. \tag{32}$$

For stability, we require the transverse Lyapunov exponents ($\lambda \neq 0$) to be negative. This is equivalent to the statement that the maximum transverse Lyapunov exponent is less than zero for each $\lambda \neq 0$:

$$\mu_{\max}(\lambda) = h_{\max} + \frac{1}{N} Re(\lambda) < 0, \quad \lambda \neq 0. \tag{33}$$

In other words, the stability zone Ω is the region defined by $\mathrm{Re}(\lambda) < -Nh_{\max}$ (see Fig. 3(a)). The distance function from the center of each Gershgörin disc to the stability boundary is given by: $\delta(G_{ii} - G_{ki}) = -Nh_{\max} - (G_{ii} - G_{ki})$ (i = 1,...,N, $i \neq k$). Thus, the kth set of stability conditions is

$$(G_{ii} - G_{ki}) < -Nh_{\max}, \tag{34}$$

$$\sum_{j=1, j\neq i}^{N} |G_{ji} - G_{ki}| < -Nh_{\max} - (G_{ii} - G_{ki}), \quad i = 1, 2, \ldots, N, \quad i \neq k. \tag{35}$$

It is obvious that the second inequality implies the first one. So the stability condition for the synchronized state is given by

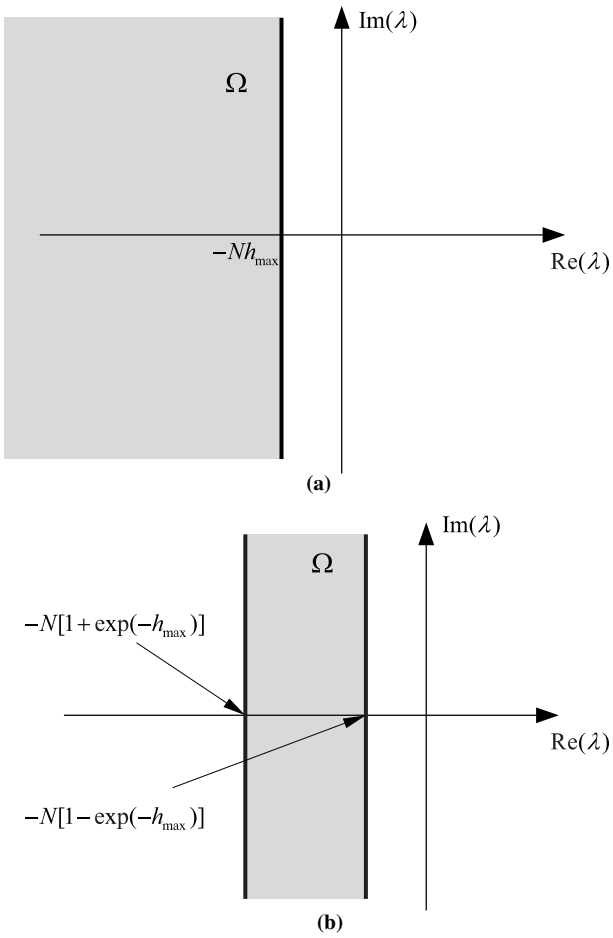

Fig. 3. Stability region of synchronized chaotic states: (a) coupled ODEs, (b) coupled maps.

$$\sum_{j=1,j\neq i}^{N} |G_{ji} - G_{ki}| + (G_{ii} - G_{ki}) < -Nh_{\max}, \quad i = 1, 2, \ldots, N, \ i \neq k. \tag{36}$$

When the coupling is symmetric, i.e. $G_{ij} = G_{ji}$, Rangarajan and Ding [44] based on the use of Hermitian and positive semidefinite matrices, derived a very simple stability constraint

$$G_{ij} > h_{\max} \quad \forall\ i, j. \tag{37}$$

We show here that Eq. (37) is a consequence of the more general stability conditions given in Eq. (36). This can be seen as follows. First consider $k = 1$. Substituting $G_{ii} = -\sum_{j=1,j\neq i}^{N} G_{ji}$ (synchronization condition for symmetric coupling) and simplifying we get the following equation:

$$\sum_{j=2,j\neq i}^{N} |G_{ji} - G_{1i}| - \sum_{j=2,j\neq i}^{N} G_{ji} - 2G_{1i} < -Nh_{\max}, \quad i \neq 1. \tag{38}$$

If $G_{ji} - G_{1i}$ is positive for all allowed i and j values, it is easy to see that the above stability condition is satisfied given the condition in Eq. (37). However, if more than two such terms are negative we have a problem. We can get around this by considering the other $(N-1)$ sets of stability conditions obtained by setting $k = 2, 3, \ldots, N$ in Eq. (36):

$$\begin{aligned}
&\sum_{j=1, j\neq i\neq 2}^{N} |G_{ji} - G_{2i}| - \sum_{j=1, j\neq i\neq 2}^{N} G_{ji} - 2G_{2i} < -Nh_{\max}, \quad i \neq 2, \\
&\vdots \\
&\sum_{j=1, j\neq i}^{N-1} |G_{ji} - G_{Ni}| - \sum_{j=1, j\neq i}^{N-1} G_{ji} - 2G_{Ni} < -Nh_{\max}, \quad i \neq N.
\end{aligned} \tag{39}$$

If we take the average of the inequalities over k, cancellation takes place, resulting in a simplified inequality. This is satisfied if the sufficient condition given in Eq. (37) is met. In other words, the previously derived stability condition is obtained as a special case when we require the coupling strengths to meet the N stability conditions simultaneously.

3.2.2. Coupled maps

In the second example, we consider a coupled map with $\mathbf{H} = \mathbf{f}$ [30,10,17,58,28]. Under this assumption, $D\mathbf{H} = \mathbf{J}$ and the linearized equation [cf. Eq. (4)] reduces to

$$\mathbf{u}(n+1) = \left(\frac{\lambda}{N} + 1\right)\mathbf{J}(\mathbf{x}(n))\mathbf{u}(n). \tag{40}$$

The Lyapunov exponents for Eq. (40) are easily calculated analytically. Denoting them by $\mu_1(\lambda), \mu_2(\lambda), \ldots, \mu_M(\lambda)$, we have

$$\mu_i(\lambda) = h_i + \ln\left|\frac{\lambda}{N} + 1\right|, \quad i = 1, 2, \ldots, M. \tag{41}$$

For stability, we require $\mu_{\max}(\lambda) = h_{\max} + \ln|\frac{\lambda}{N} + 1| < 0$ for all $\lambda \neq 0$. In other words, the stability zone (see Fig. 3(b)) is defined by

$$|\lambda + N| < N\exp(-h_{\max}), \quad \lambda \neq 0. \tag{42}$$

The distance from the center of each Gershgörin disc to the boundary is easily calculated to be $\delta(G_{ii} - G_{ki}) = N\exp(-h_{\max}) - |N + G_{ii} - G_{ki}|$ $(i = 1, \ldots, N,\ i \neq k)$. Thus, the conditions of stability are

$$\begin{aligned}
&\sum_{j=1, j\neq i}^{N} |G_{ji} - G_{ki}| + |N + (G_{ii} - G_{ki})| < N\exp(-h_{\max}), \\
&\quad i = 1, \ldots, N, \ \ i \neq k, \ \ k = 1 \text{ or } 2 \text{ or } \cdots \text{ or } N.
\end{aligned} \tag{43}$$

For each k from 1 to N, we obtain a set of sufficient stability conditions.

In [44], a simple stability bound for synchronized chaos in the case of symmetric coupling was obtained as

$$[1-\exp(-h_{\max})] < G_{ij} < [1+\exp(-h_{\max})] \quad \forall i,j. \tag{44}$$

This can again be derived from the general stability condition in Eq. (43) with the averaging technique used above.

4. Comparison of general stability constraints with exact solutions

The general stability constraints on coupling strengths derived above give sufficient conditions for the stability of the synchronized state. This is useful for those systems where necessary and sufficient conditions are hard to get. Generally speaking, the closer the sufficient condition approaches the necessary and sufficient condition, the better it is. Let us look at an example whose necessary and sufficient condition for the stability of the synchronized state can be derived analytically. By comparing this condition with our Gershgörin theory based condition, we can get some idea about how close is the approximate stability region given by Gershgörin theorem to the exact solution.

Consider a popular system of N identical maps with P nearest neighbor coupling

$$\mathbf{x}_j(n+1) = \mathbf{f}(\mathbf{x}_j(n)) + \frac{1}{2P}\sum_{p=1}^{P} a_p[\mathbf{f}(\mathbf{x}_{j+p}(n)) + \mathbf{f}(\mathbf{x}_{j-p}(n)) - 2\mathbf{f}(\mathbf{x}_j(n))], \quad j = 1,2,\ldots,N. \tag{45}$$

The coupling matrix is given by

$$\mathbf{G} = \frac{N}{2P}\begin{pmatrix} -2\sum_{p=1}^{P} a_p & a_1 & \cdots & a_P & 0 & \cdots & 0 & a_P & \cdots & a_1 \\ a_1 & -2\sum_{p=1}^{P} a_p & a_1 & \cdots & a_P & 0 & \cdots & a_P & \cdots & a_2 \\ \cdots & & & \cdots & & & & \cdots & & \\ a_1 & \cdots & a_P & 0 & \cdots & 0 & a_P & \cdots & a_1 & -2\sum_{p=1}^{P} a_p \end{pmatrix}. \tag{46}$$

This matrix is cyclic and shift invariant. Therefore, its eigenvectors have the following form [9]:

$$\mathbf{e}_l = \left(\exp\left(2\pi \mathrm{i}\frac{l}{N}\right), \exp\left(4\pi \mathrm{i}\frac{l}{N}\right), \ldots, \exp\left(2N\pi \mathrm{i}\frac{l}{N}\right)\right)^{\mathrm{T}}, \tag{47}$$

where $l = 0,1,\ldots,N-1$. Here, $l = 0$ corresponds to the synchronized case. In terms of the eigenvectors, we get the eigenvalues of the coupling matrix by the following relation:

$$\lambda_l = \frac{\mathbf{e}_l^{\mathrm{T}}\mathbf{G}\mathbf{e}_l}{\mathbf{e}_l^{\mathrm{T}}\mathbf{e}_l}, \quad l = 0,1,\ldots,N-1. \tag{48}$$

Substituting Eqs. (46) and (47) in Eq. (48), we get

$$\lambda_l = -\frac{2N}{P}\sum_{p=1}^{P} a_p \sin^2\frac{\pi p(l-1)}{N}, \quad l = 0,1,\ldots,N-1. \tag{49}$$

Recasting inequality (42) using the above expressions for eigenvalues and their symmetry, we get the following exact stability conditions:

$$\left|1-\frac{2}{P}\sum_{p=1}^{P}a_p\sin^2\left(\frac{\pi pl}{N}\right)\right|<\exp(-h_1),\quad l=0,1,\ldots,\frac{N}{2}\ \text{ or }\ \frac{N-1}{2}. \tag{50}$$

As a numerical example we consider coupled logistic maps in the chaotic regime where $f(x) = 1 - ax^2$ with $a = 1.9$. The maximum Lyapunov exponent h_1 is 0.549. For simplicity, we restrict ourselves to $N = 5$ and $P = 2$. The stability conditions for the synchronized chaotic state are

$$1-\exp(-h_1)<a_1\sin^2(\pi l/5)+a_2\sin^2(2\pi l/5)<1+\exp(-h_1), \tag{51}$$

where $l = 1, 2$. In this numerical example, the matrix **G** corresponding to our general form is the following:

$$\mathbf{G}=\frac{5}{4}\begin{pmatrix} -2(a_1+a_2) & a_1 & a_2 & a_2 & a_1 \\ a_1 & -2(a_1+a_2) & a_1 & a_2 & a_2 \\ a_2 & a_1 & -2(a_1+a_2) & a_1 & a_2 \\ a_2 & a_2 & a_1 & -2(a_1+a_2) & a_1 \\ a_1 & a_2 & a_2 & a_1 & -2(a_1+a_2) \end{pmatrix}. \tag{52}$$

Substituting in Eq. (43), we get the following sufficient conditions:

$$\left|1-\frac{1}{4}(3a_1+2a_2)\right|+\frac{1}{2}|a_1-a_2|<\exp(-h_1),$$

$$\left|1-\frac{1}{4}(2a_1+3a_2)\right|+\frac{1}{2}|a_1-a_2|<\exp(-h_1).$$

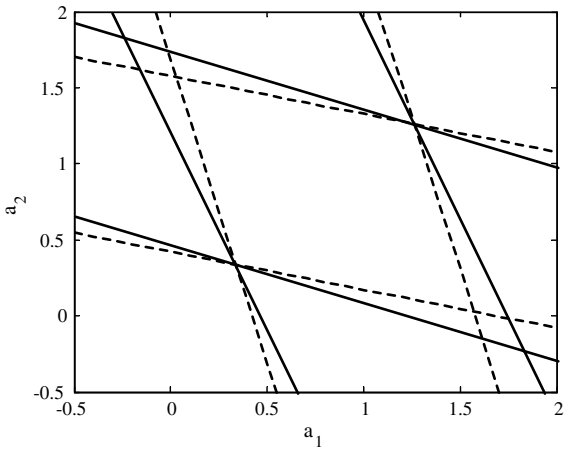

Fig. 4. Comparison of the our stability bounds (– – –) with exact bounds (—).

Simplifying the absolute values, we find the following bounds:

$$1 - \exp(-h_1) < \frac{1}{4}a_1 + a_2 < 1 + \exp(-h_1),$$
$$1 - \exp(-h_1) < a_1 + \frac{1}{4}a_2 < 1 + \exp(-h_1).$$

Comparing this sufficient condition Eq. (53) to the exact solution Eq. (51), we obtain Fig. 4 where solid lines denote the exact solution and dashed lines the sufficient condition. We see that our conditions are a very good approximation to the exact bound.

5. Pattern formation

5.1. Pattern selection

We now turn to the problem of pattern formation in coupled systems. It turns out this has an intimate connection with the stability problem we had studied in the previous sections. In the stability problem, the eigenvalues of the coupling matrix played an important role. In the study of pattern formation, the eigenvectors of the matrix play an equally important role.

Given a coupled system, using the stability bounds on coupling strengths, we selectively realize any admissible pattern we desire. This is done by destabilizing a particular eigenmode. This in turn is achieved by varying the coupling strengths such that we cross the stability boundary along a particular path. Of course, to do this accurately we need exact expressions for the stability zone boundaries. However, even the sufficient conditions that we had derived earlier can provide adequate guidance in the absence of such information. We note that our approach of obtaining stability bounds in terms of the coupling strengths makes pattern selection quite simple. Since the coupled system is specified in terms of coupling strengths, varying them to achieve pattern selection is easily done.

Equally important, our approach enables us to obtain generalizations of the classic Turing patterns. In the classic approach, the synchronized state is an equilibrium point which is destabilized to give a Turing pattern with a simple time evolution of the spatial pattern. In our case, the synchronized state can be chaotic and consequently the temporal evolution of the spatial pattern is also chaotic. Further, our couplings need not be diffusive. We call the more general spatiotemporal patterns that we obtain as Generalized Turing Patterns (GTPs).

For general couplings, the spatial pattern is not necessary a Fourier mode of the linearized system like the Turing's original case. However when the coupling matrix is shift-invariant, the eigenmodes will continue to be Fourier modes. In the following we obtain an explicit strategy for adjusting the coupling parameters to get a specific pattern. The difference in the temporal evolution of the patterns that emerge from the synchronized equilibrium points and synchronized chaotic states is also highlighted.

Let us consider a system of N identical maps with P nearest neighbor coupling whose dynamical equations are given in Eq. (45). This system has a general non-diffusive coupling which is different from the diffusive coupling used in reaction–diffusion systems. However, the coupling matrix is still shift-invariant and therefore the eigenvectors of the coupling matrix shown in Eq. (47) are the Fourier modes. Further, the inequalities (50) define a stability region in the parameter space

spanned by the coupling strengths a_p's. By selecting a given Fourier mode and choosing a suitable path in the parameter space we can realize the corresponding GTP. Note that, if one considers only the nearest neighbor ($P = 1$) diffusive coupling, the parameter space is one-dimensional and at most two GTPs can be excited by varying the coupling strengths. By enlarging the parameter space we obtain much greater variety in terms of GTPs that can be realized.

As a numerical example we consider coupled logistic maps in the chaotic regime where $f(x) = 1 - ax^2$ with $a = 1.9$. For $N = 5$ and $P = 2$, we have the stability conditions for the synchronized chaotic state given in Eq. (51). In Fig. 5(a), we exhibit the stability region marked black in the parameter plane. Next we consider the five eigenvectors [cf. Eq. (47)] which correspond to Fourier modes in this case. The eigenvector $\mathbf{e}_0$ corresponds to the synchronized state and is excluded. Of the remaining 4 eigenvectors, only 2 are independent by symmetry of Fourier modes. We take these to be $\mathbf{e}_1$ and $\mathbf{e}_2$ [cf. Eq. (47)] corresponding to $l = 1$ and 2, respectively. We call the $l = 1$ mode the long-wavelength (LW) pattern and the $l = 2$ mode the short-wavelength (SW) pattern. The arrows in Fig. 5(a) indicate paths in the parameter space which allow us to selectively destabilize one of these two modes and realize the corresponding spatial pattern.

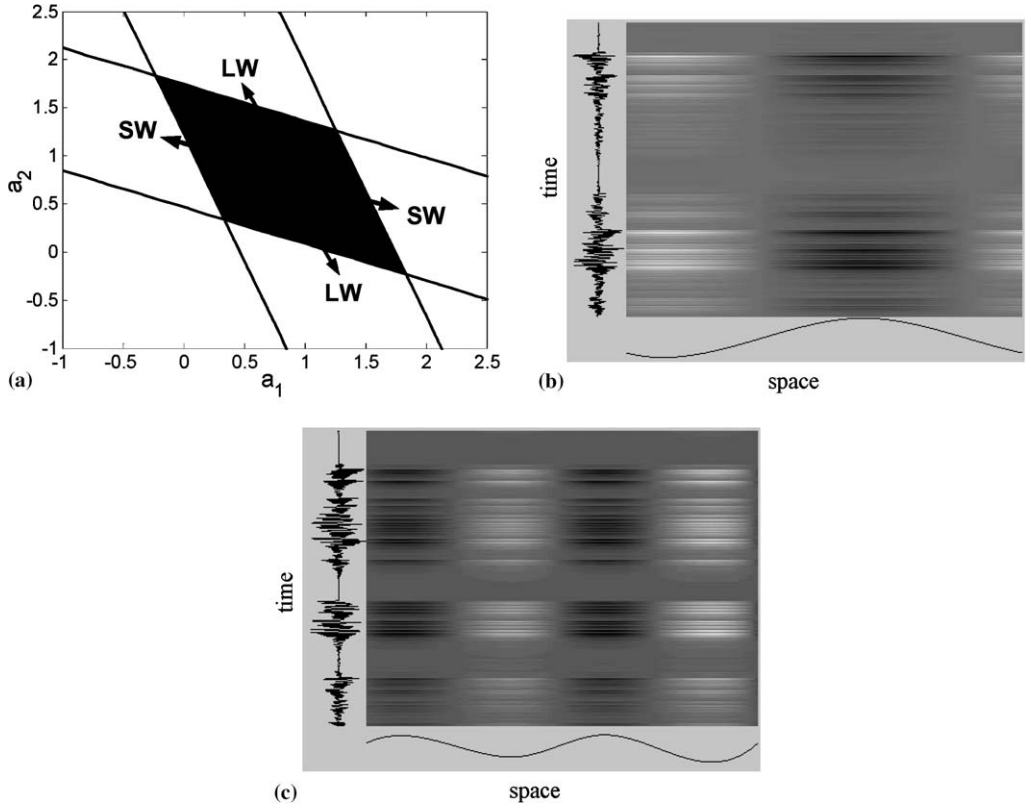

Fig. 5. Pattern selection from the synchronized chaotic state in a one-dimensional map lattice ($P = 2$). In (a) the region of stable synchronization (black area) and distinct pattern selection directions are shown. In (b) temporal evolution of the LW pattern is given with $a_1 = 0.96$, $a_2 = 0.1$. In (c) temporal evolution of the SW pattern with $a_1 = 0.04$, $a_2 = 1.1$ is given.

The main frame in Fig. 5(b) shows the temporal dynamics of the LW pattern for $a_1 = 0.96$ and $a_2 = 0.1$. Here, deviations from the synchronization manifold is approximated by

$$z_i(n) = x_i(n) - \sum_{j=1}^{N} \frac{x_j(n)}{N}, \quad i = 1, 2, \ldots, N$$

with $N = 5$. To facilitate visualization, at each time step n, a continuous function is splined through the six discrete nodes: $z_1(n)$, $z_2(n), \ldots, z_5(n)$, and $z_6(n) = z_1(n)$. Furthermore, to overcome the distortion due to the two opposite phases of a pattern, we monitor the deviation at a given node and multiply the deviations at every node by -1 whenever the deviation at the monitored node becomes negative.

Since the bifurcation undergone by the system at the boundary of the stability region is the blow-out bifurcation and there is only one attractor prior to the bifurcation, the temporal dynamics in this case is referred to as on–off intermittency [9,10,15,43]. The temporal evolution of the deviations at a typical node is given by the curve to the left of the main pattern frame. Its bursting behavior is characteristic of on–off intermittency. The GTP itself is given at the bottom of Fig. 5(b). For $a_1 = 0.04$ and $a_2 = 1.1$ we observe the SW pattern in Fig. 5(c). The same visualization methods are used to make this figure.

To understand how the synchronized state shapes the temporal properties of the GTP after desynchronization, we consider a case where the synchronized state is a fixed point. Again we use the coupled logistic maps and choose $a = 0.5$. The fixed point is $\bar{x} = 0.73$ and the Lyapunov exponent is $h_1 = -0.31$. Still letting $N = 5$, $P = 2$, from Eq. (51) we get the stability region shown in Fig. 6(a). Following the arrows we can realize either the long- or the short-wavelength patterns. Fig. 6(b) gives the LW pattern for $a_1 = 0.5$ and $a_2 = 2.5$ and Fig. 6(c) gives the SW pattern for $a_1 = 2.5$ and $a_2 = 0.5$. The same methods of plotting as that used for Fig. 1 are used here. Comparing Fig. 6(b) and (c) with Fig. 5(b) and (c) we see the same spatial patterns but different temporal behaviors.

In Fig. 6 the final GTPs are the new fixed points displayed as a function of the space coordinate. Predicting the exact location of these new fixed points requires the non-linear terms dropped in the linear stability analysis. Although it is often the case that the spatial functions underlying the new fixed points agree with the respective linear eigenmodes this is by no means a guaranteed fact [37]. On the other hand, when the synchronized state is chaotic, linear analysis will govern the temporal evolution whenever the phase space trajectory returns close to the synchronization manifold.

5.2. Design couplings using the master stability function

In the previous section, given a coupled system, we showed how to realize a specific GTP by varying the coupling strengths. In this section, we consider the inverse problem. Given a spatial pattern with a particular temporal evolution, we design a coupled system that will give this pattern when dynamically evolved.

From Eq. (3) or (6) we know that if one eigenvalue $\bar{\lambda}$ of the coupling matrix $\mathbf{G}$ is slightly outside the stable region Ω, then the deviations from the synchronized manifold along the corresponding eigenmode will grow exponentially with time and eventually giving rise to a spatial pattern when bounded by the non-linearity of the system. Therefore, we can selectively control the pattern

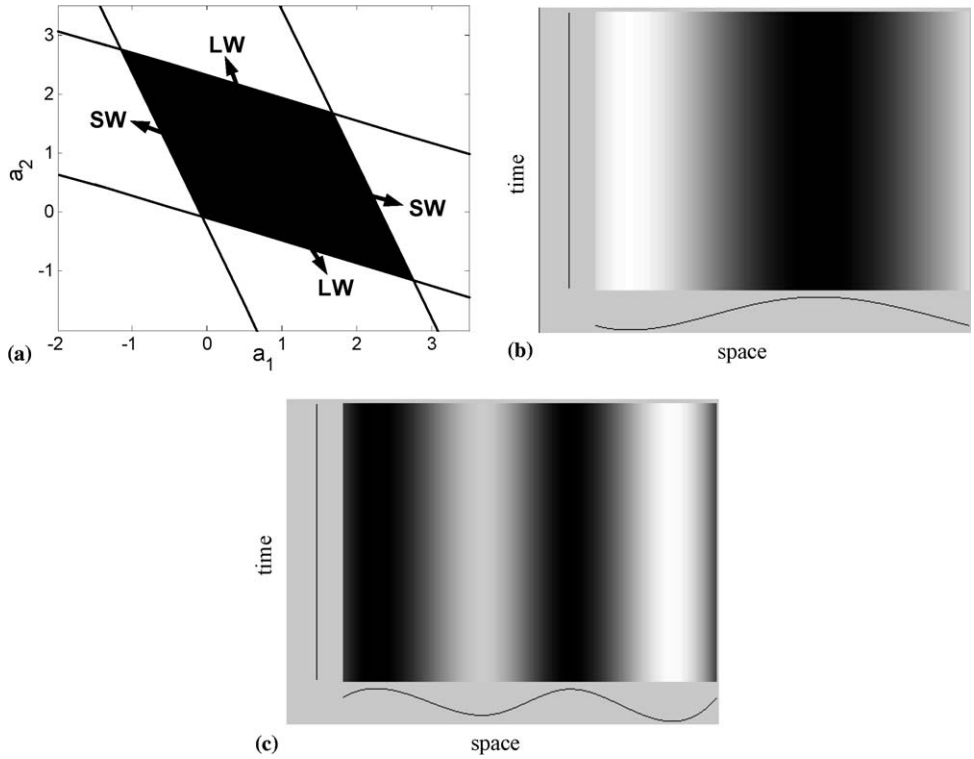

Fig. 6. Pattern selection from the synchronized equilibrium state in a one-dimensional map lattice ($P = 2$). In (a) the region of stable synchronization (black area) and distinct pattern selection directions are shown. In (b) the long-wavelength pattern evolving as a fixed point in time is given with $a_1 = 0.5$, $a_2 = 2.2$. In (c) the short-wavelength pattern with $a_1 = 2.2$, $a_2 = 0.5$ is shown.

formation of the system by making the corresponding eigenvalue fall slightly outside the stability region Ω.

On the other hand, we may want to just get a specific pattern. This pattern is given by specifying the ratios b_i/b_1 ($i = 2, 3, \ldots, N$) where b_i is the amplitude of deviation from the synchronized manifold at the ith node. For nearest neighbor coupling the patterns are fixed (the ith ratio is given by the amplitude of a cosine curve). But we want to specify an arbitrary spatial pattern. Then designing a coupled system which gives rise to such a pattern is a problem that occurs in areas such as the learning rule problem in neural networks [46]. We now outline a procedure for solving such problems:

(1) Choose the individual system unless already specified. If the temporal evolution needs to be chaotic choose the individual system to be chaotic. The number of systems that need to be coupled together is determined by the dimension N of the vector specifying the desired spatial pattern.
(2) Unless specified, choose a simple coupling function **H** that will enable easy determination of the stability region Ω.
(3) Determine the stability region Ω as described in Section 2.

(4) Design a shift-invariant $N \times N$ coupling matrix as follows. We want the desired pattern as one of the eigenvectors of the coupling matrix with its corresponding eigenvalue just outside the stability region so that it is unstable and grows exponentially. Then the spatial pattern that results from time evolution would have the same amplitude ratios as the desired pattern. One of the other eigenvectors is also specified since we start out from a synchronized state. The eigenvector is $(1 \quad 1 \quad \cdots \quad 1)^{\mathrm{T}}$ and the corresponding eigenvalue is 0. Thus, our job reduces to designing a $N \times N$ coupling matrix with the above two eigenvectors and corresponding eigenvalues. Moreover, we want the eigenvalues corresponding to the remaining $N-2$ eigenmodes to lie within the stability region so that they do not grow with time. This is ensured by constructing the eigenvalue matrix $\mathbf{\Lambda}$ and the eigenvector matrix $\mathbf{E}$ as follows. The first diagonal entry of $\mathbf{\Lambda}$ is zero (corresponding to the synchronized state) and the second diagonal entry should be chosen to lie just outside Ω. The remaining $N-2$ diagonal entries are chosen to lie within Ω. All off-diagonal entries are zero. As for $\mathbf{E}$, its first column is taken to be $(1 \quad 1 \quad \cdots \quad 1)^{\mathrm{T}}$. The desired spatial pattern constitutes the second column. The remaining $N-2$ columns are chosen randomly except that they are linearly independent to one another and to the first two columns. The coupling matrix $\mathbf{G}$ can now be formed: $\mathbf{G} = \mathbf{E}\mathbf{\Lambda}\mathbf{E}^{-1}$.

In order to make the whole process concrete, let us consider an example. The desired pattern is assumed to be $(1, -2, 3, -3, 2, -1, 1, -1, 3, -3)^{\mathrm{T}}$. To realize this, we design a $N = 10$ coupled system as follows. We choose the logistic map as the individual system with $a = 1.9$ which makes the individual system chaotic. The stability region is $-15.78 < \mathrm{Re}(\lambda) < -4.22$ according to Eq. (42). Therefore, the eigenvalue matrix can be chosen as $\mathbf{\Lambda} = \mathrm{diag}(0, -4, -6, -8, -10, -5, -9, -11, -6.5, -10.5)$. The eigenvector matrix is chosen as

$$\mathbf{E} = \begin{pmatrix} 1 & 1 & 1 & 1 & 1 & 1 & 1 & 1 & 1 & 1 \\ 1 & -2 & 3 & -3 & 2 & -1 & 1 & -1 & 3 & -3 \\ & & \text{eight} & & \text{random} & & \text{vectors} & & & \end{pmatrix}^{\mathrm{T}}.$$

Therefore, the coupling matrix $\mathbf{G}$ is

$$\mathbf{G} = \begin{pmatrix} -9.53 & 7.40 & 10.20 & 31.11 & 5.37 & -16.31 & -15.26 & 4.68 & 3.74 & -21.67 \\ -3.06 & 5.42 & 13.21 & 42.37 & 8.11 & -20.38 & -21.50 & 4.09 & 2.27 & -30.53 \\ 1.01 & 3.71 & 0.41 & 23.88 & 5.89 & -14.82 & -10.83 & 3.64 & 2.33 & -15.22 \\ -4.43 & 9.33 & 10.98 & 28.99 & 8.71 & -19.97 & -19.81 & 5.41 & 3.22 & -22.43 \\ 0.07 & 6.12 & 11.40 & 30.51 & -1.95 & -19.57 & -13.51 & 5.68 & 1.46 & -20.20 \\ -1.54 & 10.14 & 11.73 & 34.23 & 7.11 & -27.13 & -18.52 & 5.19 & 2.01 & -23.22 \\ -1.48 & 8.76 & 11.59 & 35.11 & 8.58 & -21.09 & -25.40 & 4.59 & 2.55 & -23.22 \\ -2.75 & 9.43 & 11.46 & 36.71 & 8.13 & -19.76 & -19.91 & -2.27 & 3.31 & -24.34 \\ 1.47 & 6.04 & 9.80 & 28.72 & 4.29 & -17.11 & -12.22 & 4.85 & -5.13 & -20.71 \\ -4.67 & 10.38 & 11.65 & 39.23 & 8.50 & -19.04 & -20.37 & 4.75 & 2.99 & -33.43 \end{pmatrix}.$$

Using the designed coupling matrix and simulating the dynamics, we get the desired pattern as shown in Fig. 7. The same techniques that were used in Figs. 5 and 6 have been applied to this figure.

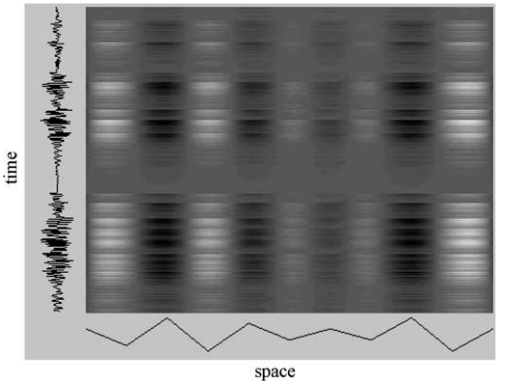

Fig. 7. The desired spatiotemporal pattern achieved by designing couplings for 10 coupled logistic maps.

6. Conclusions

In this work we described a unified framework for analyzing stability and pattern formation in coupled dynamical systems. This framework focuses on the key role played by the eigenvalues and eigenvectors of the coupling matrix. Using this framework and applying Gershgörin disc theorem to the eigenvalues of the coupling matrix, general constraints on the coupling strengths which ensure the stability of the synchronized state were obtained. Stability of both synchronized equilibrium states and synchronized chaotic states were studied for various examples. Analysis of synchronized limit cycles can be performed in a similar manner. Within the same framework we studied pattern formation in coupled systems. By destabilizing a synchronized chaotic state, we observed the emergence of generalized Turing patterns with interesting temporal evolution. Different patterns were selectively realized in a simple manner by varying the coupling strengths along a specified path in the parameter space. Finally, given a desired spatiotemporal pattern, we gave a recipe for designing a coupled system which will realize this pattern under temporal evolution.

Acknowledgment

The work was supported by US National Institutes of Health grants MH070498 and MH71620. GR was also supported by ISRO and DRDO through the Non-linear Studies Group, IISc.

Appendix A

A.1. Derivation of boundary curve

To discover the stability zone we study the eigenvalue α of the matrix $(\mathbf{J} + \frac{\lambda}{N} \cdot D\mathbf{H})$ as a function of λ. The characteristic polynomial of this matrix is given by

$$f(\alpha) = \alpha^2 + \alpha\left(a + b - \frac{\lambda}{N}\right) + \left(k_{ei}k_{ie} + ab - b\frac{\lambda}{N}\right).$$

For an arbitrary coupling matrix **G**, its eigenvalues λ could be complex:

$$\lambda = \lambda_R + \mathrm{i}\lambda_I.$$

Then the characteristic polynomial becomes

$$f(\alpha) = \alpha^2 + \alpha\left(a + b - \frac{\lambda_R}{N} - \mathrm{i}\frac{\lambda_I}{N}\right) + \left(k_{ei}k_{ie} + ab - b\frac{\lambda_R}{N} - \mathrm{i}b\frac{\lambda_I}{N}\right).$$

The range of parameter values which gives $\mathrm{Re}(\alpha) < 0$ can be determined by applying the generalized Routh–Hurwitz criterion. Following this procedure, consider $-\mathrm{i}f(\mathrm{i}\alpha)$:

$$-\mathrm{i}f(\mathrm{i}\alpha) = \mathrm{i}\alpha^2 + \alpha\left(a + b - \frac{\lambda_R}{N}\right) - \mathrm{i}\alpha\frac{\lambda_I}{N} - \mathrm{i}\left(k_{ei}k_{ie} + ab - b\frac{\lambda_R}{N}\right) - b\frac{\lambda_I}{N}.$$

This has to be put into the following standard form:

$$-\mathrm{i}f(\mathrm{i}\alpha) = b_0\alpha^2 + b_1\alpha + b_2 + \mathrm{i}[a_0\alpha^2 + a_1\alpha + a_2].$$

Comparing the two equations we get

$$a_0 = 1, \quad a_1 = -\frac{\lambda_I}{N}, \quad a_2 = -\left(k_{ei}k_{ie} + ab - b\frac{\lambda_R}{N}\right),$$

$$b_0 = 0, \quad b_1 = \left(a + b - \frac{\lambda_R}{N}\right), \quad b_2 = -b\frac{\lambda_I}{N}.$$

Applying the generalized Routh–Hurwitz criterion, we have $\mathrm{Re}(\alpha) < 0$ if the following two conditions are met:

$$\nabla_2 = \begin{vmatrix} 1 & -\frac{\lambda_I}{N} \\ 0 & \left(a + b - \frac{\lambda_R}{N}\right) \end{vmatrix} > 0$$

and

$$\nabla_4 = \begin{vmatrix} 1 & -\frac{\lambda_I}{N} & -\left(k_{ei}k_{ie} + ab - b\frac{\lambda_R}{N}\right) & 0 \\ 0 & \left(a + b - \frac{\lambda_R}{N}\right) & -b\frac{\lambda_I}{N} & 0 \\ 0 & 1 & -\frac{\lambda_I}{N} & -\left(k_{ei}k_{ie} + ab - b\frac{\lambda_R}{N}\right) \\ 0 & 0 & \left(a + b - \frac{\lambda_R}{N}\right) & -b\frac{\lambda_I}{N} \end{vmatrix} > 0.$$

Evaluating the above determinants and simplifying, we get

$$\left(a + b - \frac{\lambda_R}{N}\right) > 0,$$

$$\left(k_{ei}k_{ie} + ab - b\frac{\lambda_R}{N}\right)\left(a + b - \frac{\lambda_R}{N}\right)^2 - b\left(\frac{\lambda_I}{N}\right)^2\left(\frac{\lambda_R}{N} - a\right) > 0.$$

Solving the inequalities, the stability region Ω is found to be the region to the left of the curve

$$\lambda_I^2 = \frac{(N(k_{ei}k_{ie} + ab) - b\lambda_R)(N(a + b) - \lambda_R)^2}{b(\lambda_R - Na)}. \tag{14}$$

A.2. Derivation of shortest distance

The distance γ from the center $(G_{ii}, 0)$ of the ith Gershgörin disc to any point on the boundary of the stability zone is given by

$$\gamma^2 = (\lambda_R - G_{ii})^2 + \lambda_I^2.$$

Substituting λ_I from Eq. (14) and differentiating with respect to λ_I, we have

$$\frac{\mathrm{d}\gamma^2}{\mathrm{d}\lambda_R} = 2(\lambda_R - G_{ii}) - \frac{(N(a+b) - \lambda_R)^2}{(\lambda_R - Na)} + \frac{[(\lambda_R - Na)^2 - (Nb)^2](N(ab + k_{ie}k_{ei}) - b\lambda_R)}{b(\lambda_R - Na)^2}.$$

Setting $\frac{\mathrm{d}\gamma^2}{\mathrm{d}\lambda_R} = 0$, we get two solutions:

$$\lambda_R = Na \pm Nb\sqrt{\frac{Nk_{ie}k_{ei}}{2b[N(a+b) - G_{ii} + Nk_{ie}k_{ei}]}}.$$

Since the boundary of Ω lies to the right of the point $(\mathrm{Na}, 0)$, we can discard the smaller solution. Substituting the remaining solution in the equation for γ^2 and taking the square root, we get the shortest distance as

$$\delta_i = \gamma_{\min} = \sqrt{A_i + 2N\sqrt{B_i}}, \quad i = 1, 2, \ldots, N, \tag{53}$$

where

$$A_i = (Na - G_{ii})^2 - (Nb)^2 - 2N^2 k_{ie}k_{ei},$$
$$B_i = Nk_{ie}k_{ei}[2b(N(a+b) - G_{ii}) + Nk_{ie}k_{ei}].$$

A.3. Derivation of rightmost tip of boundary curve

Applying the Lienard–Chipart criterion on the characteristic polynomial (22), the real parts of all eigenvalues are negative if the following inequalities are satisfied:

$$\begin{aligned} &Na^2b^2 - ab\lambda + Nk_{ie}k_{ei} > 0,\\ &2Nab(a+b) - \lambda(a+b) > 0,\\ &2(a+b) > 0,\\ &\lambda^2 - 2N(a+b)^2\lambda + 4N^2(a^3b + 2a^2b^2 + ab^3 - k_{ie}k_{ei}) > 0. \end{aligned} \tag{54}$$

Since a, b are positive, the third inequality is automatically satisfied. After simplification, the first two inequalities become

$$\lambda < N\frac{k_{ie}k_{ei} + a^2b^2}{ab},$$
$$\lambda < 2Nab.$$

The last inequality is of the form

$$a_1\lambda^2 - a_2\lambda + a_3 > 0,$$

where

$$a_1 = 1, \quad a_2 = 2N(a+b)^2, \quad a_3 = 4N^2[ab(a+b)^2 - k_{ie}k_{ei}].$$

Note that a_1, a_2 are obviously positive. It turns out a_3 is also positive because of the local stability condition derived in Eq. (21). The quadratic function $a_1\lambda^2 - a_2\lambda + a_3$ with a_1, a_2, a_3 positive has a unique global minimum at $\lambda = a_2/2a_1$. Thus, the minimum occurs at a positive value of λ. It is also seen that

$$a_2^2 - 4a_1a_3 = 4(a+b)^4[(a+b)^4 - 4[ab(a+b)^2 - k_{ie}k_{ei}]].$$

This can be simplified as

$$a_2^2 - 4a_1a_3 = 4(a+b)^4[(a^2-b^2)^2 + 4k_{ie}k_{ei}],$$

which is positive since $k_{ie}k_{ei}$ is positive. Thus, both the zeros of the quadratic function (we will denote them η_1 and η_2 with $\eta_1 < \eta_2$) are real. Further, since $a_3 > 0$ and the global minimum occurs at a positive value, $\eta_2 > \eta_1 > 0$. Consequently, the last inequality is satisfied when $\lambda < \eta_1$ or $\lambda > \eta_2$ where

$$\eta_{1,2} = N(a+b)^2 \pm N\sqrt{(a+b)^4 - 4[ab(a+b)^2 - k_{ie}k_{ei}]}.$$

Note that η_1 is explicitly seen to be positive by applying Eq. (21). Further, $\eta_2 > N(a+b)^2 > 2Nab$. Thus, the inequality $\lambda > \eta_2 > 2Nab$ is not possible given the stability condition $\lambda < 2Nab$ derived earlier. Therefore, the last inequality in Eq. (54) reduces to $\lambda < \eta_1$.

Summarizing, we get the following set of stability conditions:

$$\lambda < N\frac{k_{ie}k_{ei} + a^2b^2}{ab},$$
$$\lambda < 2Nab,$$
$$\lambda < \eta_1.$$

Let $\kappa = \min\{N\frac{k_{ie}k_{ei}+a^2b^2}{ab}, 2Nab, \eta_1\}$, then all these inequalities will be simultaneously satisfied if $\lambda < \kappa$.

Thus, the rightmost tip of the boundary curve along the real axis is $(\kappa, 0)$.

References

[1] Baird B. Bifurcation and category learning in network models of oscillating cortex. Physica D 1990;42(1–3):365–84.
[2] Belykh VN, Belykh IV, Hasler M. Hierarchy and stability of partially synchronous oscillations of diffusively coupled dynamical systems. Phys Rev E 2000;62(5):6332–45.
[3] Belykh VN, Belykh IV, Mosekilde E. Cluster synchronization modes in an ensemble of coupled chaotic oscillators. Phys Rev E 2001;63:036216.
[4] Bresloff PC. Mean-field theory of globally coupled integrate-and-fire neural oscillators with dynamic synapses. Phys Rev E 1999;60(2):2160–70.

[5] Brown R, Rulkov NF. Designing a coupling that guarantees synchronization between identical chaotic systems. Phys Rev Lett 1997;78(22):4189–92.
[6] Bunimovich LA, Sinai YaG. Spacetime chaos in coupled map lattices. Nonlinearity 1988;1(4):491–516.
[8] Chen Y, Rangarajan G, Ding M. General stability analysis of synchronized dynamics in coupled systems. Phys Rev E 2003;67:026209.
[9] Ding M, Yang W. Observation of intermingled basins in coupled oscillators exhibiting synchronized chaos. Phys Rev E 1996;54(3):2489–94.
[10] Ding M, Yang W. Stability of synchronous chaos and on–off intermittency in coupled map lattices. Phys Rev E 1997;56(4):4009–16.
[11] Filatrella G, Straughn B, Barbara P. Emission of radiation from square arrays of stacked Josephson junctions. J Appl Phys 2001;90(11):5675–9.
[12] Fink KS, Johnson G, Carroll TL, Mar D, Pecora LM. Three coupled oscillators as a universal probe of synchronization stability in coupled oscillator arrays. Phys Rev E 2000;61(5):5080–90.
[13] Freeman WJ. Mass action in the nervous system. New York: Academic Press; 1975.
[14] Fujisaka H, Yamada T. Stability theory of synchronized motion in coupled oscillator systems. Prog Theor Phys 1983;69(1):32–47.
[15] Fujisaka H, Yamada T. A new intermittency in coupled dynamical systems. Prog Theor Phys 1985;74(4):918–21.
[16] Gantmacher FR. Theory of matrices. New York: Chelsea; 1964.
[17] Gauthier DJ, Bienfang JC. Intermittent loss of synchronization in coupled chaotic oscillators: toward a new criterion for high-quality synchronization. Phys Rev Lett 1996;77(9):1751–4.
[18] Glendinning P. The stability boundary of synchronized states in globally coupled dynamical systems. Phys Lett A 1999;259(2):129–34.
[19] Golub GH, Van Loan CF. Matrix computations. Baltimore: Johns Hopkins University Press; 1996.
[20] Hansel D, Sompolinsky H. Synchronization and computation in a chaotic neural network. Phys Rev Lett 1992; 68(5):718–21.
[21] Hansel D. Synchronized chaos in local cortical circuits. Int J Neural Syst 1996;7(4):403–15.
[22] Heagy JF, Pecora LM, Carroll TL. Synchronous chaos in coupled oscillator systems. Phys Rev E 1994;50(3): 1874–85.
[23] Heagy JF, Pecora LM, Carroll TL. Short wavelength bifurcations and size instabilities in coupled oscillator systems. Phys Rev Lett 1995;74(21):2188–4185.
[24] Hirsch MW, Smale S. Differential equations, dynamical systems, and linear algebra. New York: Academy Press; 1974.
[25] Hirsch MW. Convergent activation dynamics in continuous time networks. Neural Networks 1989;2(5):331–49.
[26] Horn RA, Johnson CR. Matrix analysis. Cambridge: Cambridge University Press; 1985.
[27] Hu G, Yang J, Liu W. Instability and controllability of linearly coupled oscillators: eigenvalue analysis. Phys Rev E 1998;58(4):4440–53.
[28] Jost J, Joy MP. Spectral properties and synchronization in coupled map lattices. Phys Rev E 2002;65:016201.
[30] Kaneko K. Lyapunov analysis and information flow in coupled map lattices. Physica D 1986;23(1–3):436–47.
[31] Kocarev L, Parlitz U. Generalized synchronization, predictability, and equivalence of unidirectionally coupled dynamical systems. Phys Rev Lett 1996;76(11):1816–9.
[32] Li Z, Hopfield JJ. Modeling the olfactory bulb and its neural oscillatory processings. Biol Cybernet 1989;61(5): 379–92.
[33] Li R, Erneux T. Stability conditions for coupled lasers—series coupling versus parallel coupling. Opt Commun 1993;99(3–4):196–200.
[34] Li R, Erneux T. Bifurcation to standing and traveling waves in large arrays of coupled lasers. Phys Rev A 1994; 49(2):1301–12.
[35] Li Z. Computational design and nonlinear dynamics of a recurrent network model of the primary visual cortex. Neural Comput 2001;13(8):1749–80.
[36] Munuzuri AP, Chua LO. Stationary structures in a discrete bistable reaction–diffusion system. Int J Bifurc Chaos 1997;7(12):2807–25.
[37] Murray JD. Mathematical biology. Berlin: Springer; 1993.

[38] Oppo GL, Kapral R. Domain growth and nucleation in a discrete bistable system. Phys Rev A 1987;36(12): 5820–31.
[39] Otsuka K, Kawai R, Hwong S, Ko J, Chern J. Synchronization of mutually coupled self-mixing modulated lasers. Phys Rev Lett 2000;84(14):3049–52.
[40] Pasemann F. Synchronized chaos and other coherent states for two coupled neurons. Physica D 1999;128(2–4): 236–49.
[41] Pecora LM. Synchronization conditions and desynchronizing patterns in coupled limit-cycle and chaotic systems. Phys Rev E 1998;58(1):347–60.
[42] Pecora LM, Carroll TL. Master stability functions for synchronized coupled systems. Phys Rev Lett 1998;80(10): 2109–12.
[43] Platt N, Spiegel EA, Tresser C. On–off intermittency: a mechanism for bursting. Phys Rev Lett 1993;70(3):279–82.
[44] Rangarajan G, Ding M. Stability of synchronized chaos in coupled dynamical systems. Phys Lett A 2002;296(4–5): 204–9.
[45] Rangarajan G, Chen Y, Ding M. Generalized Turing patterns and their selective realization in spatiotemporal systems. Phys Lett A 2003;310:415–22.
[46] Rojas R. Neural networks—a systematic introduction. Berlin: Springer-Verlag; 1996.
[47] Roy R, Thornburg Jr KS. Experimental synchronization of chaotic lasers. Phys Rev Lett 1994;72(13):2009–12.
[48] Rulkov NF, Sushchik MM. Robustness of synchronized chaotic oscillations. Int J Bifurc Chaos 1997;7(3):625–43.
[49] Truccolo WA, Rangarjan G, Chen Y, Ding M. Analyzing stability of equilibrium points in neural networks: a general approach. Neural Networks 2004;16:1453–60.
[50] Turing AM. The chemical basis of morphogenesis. Phil Trans Roy Soc B 1952;237(64):37–72.
[51] Waller I, Kapral R. Synchronization and chaos in coupled nonlinear oscillators. Phys Lett A 1984;105(4–5):163–8.
[52] Wersing H, Beyn W-J, Ritter H. Dynamical stability conditions for recurrent neural networks with unsaturating piecewise linear transfer functions. Neural Comput 2001;13(8):1811–25.
[53] Wilson H, Cowan JD. Excitatory and inhibitory interactions in localized populations of model neurons. Biophys J 1972;12(1):1–24.
[54] Winful HG, Rahman L. Synchronized chaos and spatiotemporal chaos in arrays of coupled lasers. Phys Rev Lett 1990;65(13):1575–8.
[55] Wu CW, Chua LO. A unified framework for synchronization and control of dynamical systems. Int J Bifurc Chaos 1994;4(4):979–98.
[56] Wu CW, Chua LO. Synchronization in an array of linearly coupled dynamical systems. IEEE Trans Circuits Syst I 1995;42(8):430–47.
[57] Zhan M, Hu G, Yang J. Synchronization of chaos in coupled systems. Phys Rev E 2000;62(2):2963–6.
[58] Zhu K, Chen T. Controlling spatiotemporal chaos in coupled map lattices. Phys Rev E 2001;63:067201.
[59] Ott E, Sommerer JC. Blowout bifurcations: the occurrence of riddled basins and on–off intermittency. Phys Lett A 1994;188:39–47.
[60] Ashwin P, Buescu J, Stewart I. Bubbling of attractors and synchronisation of chaotic oscillators. Phys Lett A 1994; 193:126–39.
[61] Venkataramani SC, et al. Transitions to bubbling of chaotic systems. Phys Rev Lett 1996;77:5361–4.
[62] Venkataramani SC, et al. Classical diffusion on Eden trees. Phys Rev Lett 1996;54:1346–9.